7. IMAGING SECONDARY ION MASS SPECTROMETRY

WILLIAM A. LAMBERTI

1. SECONDARY ION MASS SPECTROMETRY AND NANOTECHNOLOGY

Imaging secondary ion mass spectrometry ("SIMS") is a technique that holds great potential for use in the field of nanotechnology. In much the same way that focused ion beam tools evolved to become a critical capability in the fabrication of many nano-mechanical devices, SIMS is becoming a central characterization tool within the nanotechnology community. For example within the semiconductor industry, SIMS employed at low incident ion energy is now used routinely to obtain trace information from extremely thin (1 nm) layered structures in depth, albeit in the non-imaging mode of analysis [1, 2]. Imaging SIMS lateral resolution, when employing high sensitivity primary ion species, has historically been limited to 1000 nm. This disparity in lateral resolution versus depth resolution can lead to measurement difficulties when analyzing fine structures in three dimensions. However, recent instrumental developments in ion sources and SIMS ion optics have dramatically improved lateral resolution to the regime below 100 nm while maintaining high sensitivity [3]. Due to the higher primary ion energies typically employed in these high lateral resolution instruments, depth resolution is somewhat degraded, typically on the order of 10 nm. As a result, SIMS image and depth resolutions have now converged to the point where the analyst can now routinely obtain information from nanovolumes.

The application of Imaging SIMS to mainstream nanotechnology areas such as nanosensors and micro-electromechanical systems ("MEMS") has been scarce to date. This can largely be attributed to a number of factors, including instrument

availability, cost, and performance. There is also an inherent need for a highly skilled SIMS analyst. However, many examples of SIMS applications exist that do indeed qualify as examples of nano-analyses within fields as diverse as semiconductor technology, biology, metallurgy, catalysis, and cosmochemistry [4].

Many novel, *indirect*, SIMS analyses have been possible that provide information from regions that are smaller than the classical image resolution limit of SIMS (i.e. 1000 nm). The fundamental SIMS sputtering process, where a single primary ion impacts a surface and produces secondary ions, is inherently highly-localized (<5 nm radius) [5, 6]. Additionally, the probability that molecular ions are produced from a single impact is directly related to the nearest-neighbor distribution of species at the point of impact. Phenomena such as these can be used to obtain nano-scale information from materials without actually determining the precise event position with a resolution better than 1000 nm. Examples of methods utilizing this approach include coincidence spectroscopy [7, 8] and dynamic SIMS molecular spectroscopy [9].

The advantage of modern imaging SIMS instruments is that one can now *directly* probe sub 100 nanometer-scale features for compositional information, while maintaining trace sensitivity (several ppm) in these nano-volumes. The inherent ability of SIMS to detect *any* elemental species is a powerful capability for understanding the overall chemistry of a given material. Isotopic speciation is also possible with the high-resolution mass spectrometers incorporated into many SIMS instruments. Stable isotope tagging of reactant molecules permits the determination of reaction locales with high spatial resolution via SIMS, and is finding application in fields such as biology, medicine, and catalysis [10].

2. INTRODUCTION TO SECONDARY ION MASS SPECTROMETRY

2.1. Overview

The SIMS process is shown schematically below (figure 1). A beam of primary ions is generated in a suitable ion source, and accelerated towards a sample surface under vacuum. The interaction between the primary ion and the sample is complicated in nature, with many secondary particles being ejected for each incident ion. This process is referred to as "sputtering" [11, 12]. Electrons, neutral atoms, molecular fragments, and ions are generated in the sputtering process. Ionized mass fragments (monatomic and polyatomic) are subsequently accelerated through a mass spectrometer, where each fragment is separated according to its mass to charge ratio ("m/z"). Detection of the mass fragments then occurs via electron multiplier, faraday cup, or other suitable charged-particle detector. Mass spectra and ion images are among the types of data then produced.

Ion images can be produced via raster of the primary beam and synchronous detection of the mass filtered secondary ion signal, analogous to the process employed in scanning electron microscopy. This mode is referred to as the *microprobe mode* of ion imaging. It is important to note that in microprobe mode, image resolution is largely dependent upon primary ion probe diameter, with submicron lateral resolution now routinely attainable.

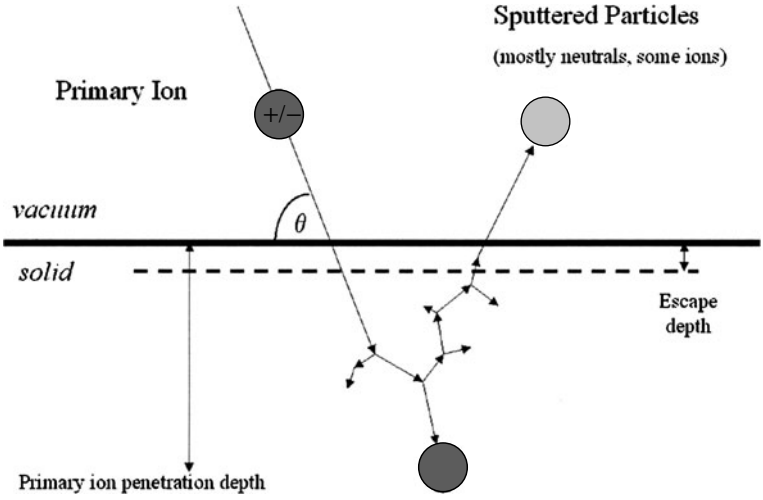

Figure 1. Schematic of the SIMS sputter process.

An alternative mode of image formation is available in some instruments known as the *microscope or direct mode* of ion imaging. The microscope mode is non-raster based, and utilizes electrostatic ion lenses in the secondary ion column. These lenses enable the formation of image planes and crossover points in the ion optical path. For final mass filtered image formation, the image planes are projected onto a position-sensitive detector. Several types of position sensitive detectors are in use today. Most commonly, a micro-channel plate coupled to a phosphor screen, with the resulting image captured by use of a suitable high-sensitivity CCD. Alternatively, ion images can be captured by use of a direct ion-imaging detector such as the resistive anode encoder ("RAE"). In microscope mode imaging, the image resolution is essentially dependent upon the ion optical lenses and their corresponding electric field strengths. In practice, image resolution is limited to roughly 1000 nm.

The choice of primary ion species will determine the efficiency of generation of specific secondary ion species, and subsequent experimental sensitivity. Primary ion energy will determine the subsequent spatial resolution in a given analysis, with lower energies favoring reduced surface mixing due to sputtering, thus improving depth resolution. However, higher primary ion beam energy can result in improved lateral resolution when in the microprobe mode.

Typical primary ion species include cesium (Cs^+), oxygen (O_2^+ or O^-), and gallium (Ga^+) with incident energies in the range of a few hundred eV to several keV. Cesium and oxygen primary beams provide significantly enhanced production of secondary ions due to the chemical interaction of each primary species with the sample surface. When used as a primary ion, oxygen enhances the production of positive secondary ions. This results from the increased oxygen concentration in the near-surface region as sputtering proceeds. This implanted oxygen tends to form metal-oxygen bonds,

which when subsequently broken due to further sputtering, tend to leave the oxygen (high electron affinity) with a net negative charge and the counter ion with a net positive charge. Cesium favors the production of negative secondary ions, largely due to a reduction in the workfunction of the surface species as cesium is implanted in the sputtering process. This reduction in workfunction permits more electrons to exist in excited states above the surface potential energy barrier. This increased availability of excited electrons within the surface then favors the production of negative ions [13, 14, 15].

The SIMS process itself remains only partly understood at the fundamental level. Molecular simulations, coupled with experimental observations continue to provide new insights into the mechanisms underlying sputtering, ionization, and subsequent detection of secondary ions [16, 17]. As with many techniques, there are potential pitfalls, artifacts and quantification difficulties with SIMS. However, it remains a very powerful tool for the determination of nano-phase compositions in materials. A complete, detailed discussion of the entire SIMS process is beyond the scope of this text. However, the reader is referred to several excellent references in the field [18, 19, 20].

2.2. General SIMS Instruments

From the perspective of instrumentation, SIMS can be categorized into one of two possible regimes: dynamic SIMS or static SIMS. The simplest distinction between dynamic and static SIMS is based upon relative sputter rates. Dynamic SIMS involves the use of high fluxes of incident primary ions, with relatively rapid removal of the atomic layers in the sample being analyzed. Much molecular information is lost in the dynamic SIMS process due to the high primary ion flux. The high ion flux can also increase surface roughening and loss of interface resolution as the analysis proceeds in depth. Nonetheless, many structures can be probed in-depth readily, albeit with only limited molecular information preserved.

Static SIMS, on the other hand, refers to the sampling of only a fraction (less than 0.1%) of the topmost monolayer of a sample's surface. Very few incident primary ions impact the sample, so very few molecular bonds are broken. All information stems from the near-surface region of the sample, with extensive molecular information possible [21]. It is worth noting that recent developments in primary ion sources utilizing multiply-charged or cluster ions have blurred some of the distinctions between these regimes in specialized cases [22, 23, 24]. In practice, for the analysis of organics with a need for molecular information, static SIMS is preferred, while dynamic SIMS usually provides the ultimate in trace elemental detection sensitivity (ppb) and spatial resolution.

Each of these regimes also tends to determine the choice of preferred mass spectrometer type. The lower secondary ion flux generated in Static SIMS molecular studies require the use of a full-spectrum mass analysis (simultaneous detection and no lost ions), and high transmission as provided by a time-of-flight ("TOF") mass spectrometer. In fact, the use of TOF spectrometers has become almost synonymous with static SIMS, which is often referred to as TOF-SIMS. High-performance,

commercial versions of these instruments include the Ion-TOF 5 [25] and Phi-Trift III [26]. The mass resolution (M / delta M) of a TOF spectrometer is dependent upon the temporal resolution of the secondary ion burst coming from the sample. This burst originates from a pulsed primary ion burst, so the temporal quality of primary ion pulse (in a process known as "bunching") defines the achievable mass resolution in an analysis. Pulsing of the primary beam is done with a duty factor of roughly 10^{-5}, and material removal is intentionally extremely slow. Unfortunately, a compromise often must be reached between mass resolution, spatial resolution, and compositional sensitivity. In some cases, TOF-SIMS lateral resolution can be below 1000 nm and may be quite appropriate for the study of certain nanostructures. This is especially true if organic molecular information is desired from such structures in the topmost surface layers. The choice of SIMS technique obviously depends upon the scientific question at hand. Issues of spatial resolution, surface versus bulk, detection sensitivity, and molecular versus elemental information must be carefully considered.

Dynamic SIMS analysis can, in principle, also be carried out using a TOF spectrometer, but is more often performed using a magnetic sector mass spectrometer with 100% duty cycle (Mattauch-Herzog configuration being common [27]), or a quadrupole mass spectrometer. Quadrupole mass spectrometers suffer from relatively poor mass resolution and transmission, but are generally less expensive and more compact. Magnetic sector instruments can simultaneously possess very high mass resolution and high transmission. The additional advantage of a non-TOF instrument, in the case of microprobe imaging, is that mass resolution and transmission can be maintained independently of image resolution. This result stems from the fact that the primary beam need not be pulsed to provide mass resolution, thus avoiding defocusing effects on the primary beam. The benefit of de-coupling these analytical parameters is significant in practice, as one can now independently optimize each portion of the instrument to serve its respective function. For example ion source design, primary ion species, and primary ion probe size can all be optimized to produce the best possible combination of sensitivity and image resolution for the analysis without impacting mass spectrometer performance.

2.3. High Resolution Imaging SIMS Instruments

It may be inferred from the previous discussion that imaging SIMS instruments with the highest spatial resolution and sensitivity tend to be magnetic sector based, dynamic SIMS instruments. Early attempts at optimizing spatial resolution on such instruments utilized highly focussed gallium (40 keV Ga+) primary ion beams [28]. Early commercial focussed ion beam ("FIB") instruments utilized gallium ion beams and added a quadrupole mass spectrometer to the FIB in the hopes of producing a useful high resolution imaging SIMS [29]. In fact, the use of gallium as a primary ion species in these instruments resulted in superb image resolution on the order of 10–20 nm. However, gallium produces extremely poor secondary ion yields for most species, resulting in poor SIMS sensitivity.

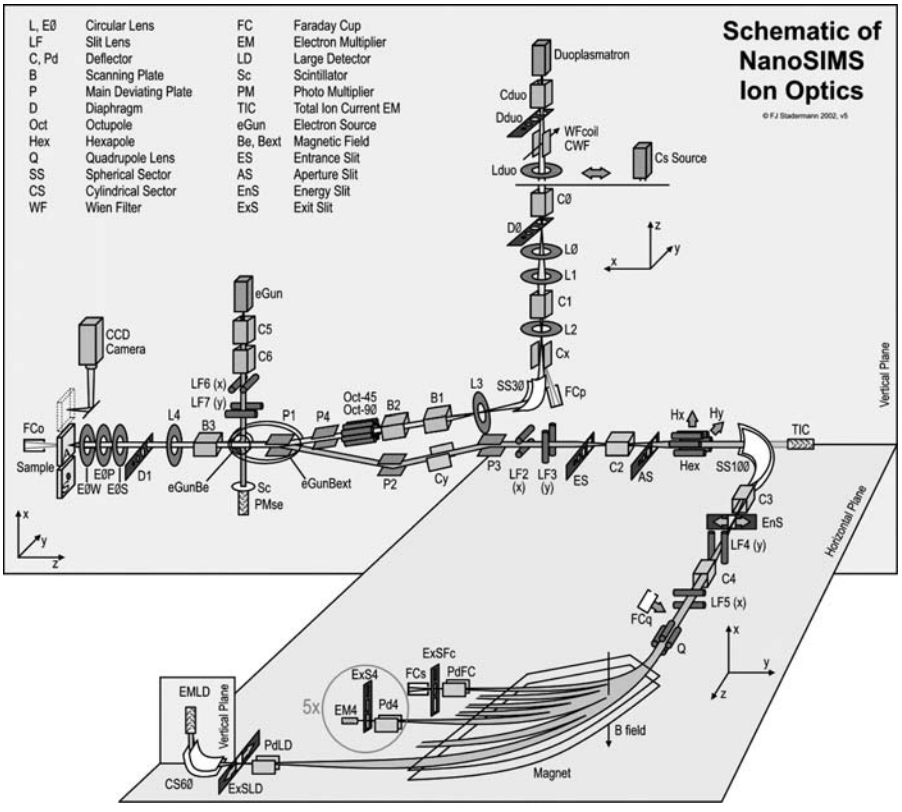

Figure 2. Schematic of ion optics for Cameca NanoSims 50. Based upon first series of commercial instruments. [reprinted with permission from F. J. Stadermann, Washington University at St. Louis. © F. J. Stadermann] (See color plate 3.)

The next major development in high resolution imaging SIMS emerged as the NanoSIMS 50 ("N50") a magnetic sector based, microprobe instrument utilizing nano-focussed cesium and oxygen ion sources [30]. Conceived in the early 1990's, the instrument design evolved over several years, with the first commercial instrument being installed in 2001. The N50 is uniquely designed for high transmission, high mass resolution, high sensitivity and high spatial resolution (50 nm), providing arguably the best overall imaging SIMS performance to date. A schematic of the N50 ion optics is provided in figure 2.

Several design features contribute to the high performance of this instrument. For example, the primary ion beam strikes the sample at normal incidence, permitting a very short distance between the sample and the probeforming lens. This geometry results in greatly reduced probe aberrations, and improved lateral resolution. Additionally, the sample is immersed in a very high electric field, facilitating efficient capture

of secondary ions (i.e., a higher useful yield). The spectrometer design provides high mass resolution (M / delta (M) = 3000 minimum) without the use of beam stops. With beam stops used, mass resolution can readily exceed 10,000 while still maintaining high transmission.

One of the drawbacks of a magnetic sector instrument compared to a TOF instrument is serial mass species detection. This limitation is addressed in the N50 design by the use of multiple, parallel ion detectors that can be independently positioned at the exit of the mass spectrometer. The latest design employs seven ion detectors, along with ion-induced secondary electron imaging (when in the negative ion collection mode) [31, 32].

The ultimate spatial resolution of the N50 is typically better than 50 nm when using the cesium primary beam, and 150 nm when using the oxygen primary beam. Each primary ion species is chosen to maximize the sensitivity for detection of a particular secondary ion. As a primary ion, cesium enhances the yield of electronegative species, while oxygen tends to enhance the yield of electropositive species [33]. Thus these two primary ion sources together effectively span the entire periodic table with ppm to ppb detection limits.

3. EXPERIMENTAL ISSUES IN IMAGING SIMS

Many issues exist in SIMS analyses that can limit the ability to quantify a result in absolute terms. In some cases, even qualitative analysis is not possible. Examples of issues one may encounter include:

- Sputter rates can vary significantly for multi-phase or polycrystalline samples, from one phase to the next, even under conditions of constant and uniform primary ion beam flux.
- Matrix effects, due to differences in local chemical environment, can cause secondary ion yields to vary dramatically (by several orders of magnitude).
- Surface roughening can occur as sputtering proceeds, resulting in loss of interface resolution.
- For polycrystalline samples, grain orientation effects can lead to variable secondary ion yields due to different amounts of primary ion channeling in each grain.
- Sample charging can make an analysis completely impossible in the worst cases, and unpredictable in some others.
- Re-deposition of sputtered material onto the analysis area, during the sputter process, can cause high background levels in some situations.
- Sample preparation and handling can have significant effects on a given SIMS measurement.

Given these issues, many analyses are still, in fact, approachable. Many quantification schemes have been developed for SIMS analysis. A summary of the major SIMS quantification methods is given in Table 1. While not exhaustive, a few of the more typical

Table 1. Summary of Major SIMS Quantification Schemes

Method	Reported Error Range (+/−)	Benefits	Drawbacks
Relative Sensitivity Factor ("RSF") [31]	10–50%	Simple to employ on well-defined systems.	- Sample matrix must be constant and well-known. - Initial standards limit accuracy of subsequent analyses.
Ion-Implanted Internal Standard [32, 33, 34]	5–50%	Can be used for any species. Sample and standard are always analyzed together.	- Standards must be generated via ion implantation for each analysis. - Sample damage can occur during implantation.
Matrix Isotope Species Ratio ("MISR") [38]	3–50%	Convenient to use on homogenous samples.	- Sample heterogeneity limits accuracy. - Calibration curves need to be generated for each sample type. - Only accounts for oxide matrix effect.
CsM^+ Cluster ("CsM^+") [46, 47, 48]	10% (w/stds) 50% (w/o stds)	Relatively insensitive to most matrix effects.	- Poor sensitivity due to low signals. - Difficult on insulators.
Infinite Velocity ("IVM") [49, 50, 51]	10–300%	No standards required.	- Not useful on insulators. - High error range

methods are briefly introduced below. A more complete discussion of each method can be found within the referenced sources.

As an example, often the analysis can be facilitated through the use of external standards developed for the system of interest. Relative sensitivity factors ("RSF's") are then determined for individual species in a given matrix. This is the approach used within much of the semiconductor industry for depth profile interpretation in well-known matrices [34].

Quantitative results can also be obtained with the use of an internal standard for each analyzed area. This introduction of an internal reference can be accomplished by a variety of methods, including ion implantation [35, 36, 37] or by physically mounting a reference standard alongside the sample in each analysis area. The use of a physically separate reference standard has been used with success, for example, in the study of trace alloying elements in steels. Utilizing a reference alloy sample to be used as a relative comparison to the sample being analyzed within each field of view, imaging SIMS analysis was performed on both the reference and unknown simultaneously. This approach resulted in a very precise (<5%) relative determination of trace boron (1–10 ppm) since each analysis of reference versus unknown was done under identical conditions of instrumental alignment and primary beam dose. Useful relative compositional information can often be obtained using this method, with final measurement accuracy limited largely by the accuracy of the internal standard [38].

The method of standard additions can also be employed, via methods such as ion implantation over a range of concentrations, to establish the analytical response for a particular species within a given matrix or sample type. Implantation of minor isotopes can be used to minimize interference from naturally occurring levels in the standards [39].

The approach known as the matrix ion species ratio method ("MISR") [40] also utilizes external standards as a means to calibrate an instrument's sensitivity for a given species, in a given matrix. The MISR method attempts to account for local matrix effects (due to variable amounts of oxygen in the sample matrix).

This is accomplished by measuring the secondary ion signal from a series of standards, as a function of partial pressure of oxygen near the sample surface. Oxygen partial pressure is controlled via an imposed oxygen gas bleed. In the MISR approach, one monitors the production of two matrix species signals as well as the species of interest. In the case of a ferrous NBS-662 steel alloy [41] the authors monitored the ratio $^{112}Fe_2{}^+/^{54}Fe^+$ as well as the species to be calibrated ($^{52}Cr^+$). The ratio of the *molecular* iron fragment to the *monatomic* fragment is very sensitive to oxygen pressure, and thus provides a means to correlate the Cr^+ sensitivity factor to the local oxygen concentration at the sample surface. The $^{112}Fe_2{}^+/^{54}Fe^+$ ratio in an "unknown" sample thus is a direct means to determine the appropriate Cr^+ sensitivity factor. Here the "unknown" still must be nominally of the same composition as the calibrant.

Another approach that can be useful when absolute standards are not possible to obtain involves simply comparing samples on a relative basis. The analyst may make very reproducible measurements within a series of samples for trends that correlate with performance. For example, quantitative SIMS image analysis of heterogeneous catalysts is possible using a statistical, image-based approach when analyzing large numbers of catalyst particles [42, 43]. Here, many catalyst particles are analyzed via imaging SIMS with subsequent multi-particle image analysis. Sufficient numbers of catalyst particles are analyzed so that the mean of the SIMS ion intensity distribution approaches a statistically valid estimate of the bulk concentration for each species. Bulk concentration values can then be used to calculate an individual catalyst particle's concentration for a particular species.

An effective approach for obtaining relative quantitative information in biological structures via SIMS involves the use of isotopically tagged molecules. While not directly used for determining absolute concentrations, the distribution and quantity of isotopically tagged molecules can be determined by mapping the appropriate isotope ratio (15 N/14 N, for example). This method works well even for samples with extreme topography or sample charging due to the fact that all isotopes of a given species will experience essentially the same effects. In these experiments, the enhancement of a minor isotope over its naturally occurring abundance has been used directly to identify, for example, the uptake of a tagged molecule towards a particular biological structure in living organisms. Any observed increase is then used to quantify the relative growth or repair rate of that particular biological structure versus the surrounding tissue [44, 45].

In summary, many issues need to be considered in a given SIMS analysis to ensure that meaningful results are obtained. However, extensive experience exists within the

SIMS literature, so very often an answer exists to most of the problems encountered. Creativity and careful experimental design are often the key to a successful analysis.

4. APPLICATIONS IN NANOTECHNOLOGY

As stated previously, the use of SIMS for the determination of nanophase information is well established in classical SIMS application areas such as semiconductor technology, catalysis, cosmochemistry, biology and materials science. These studies serve as excellent examples of what may be possible for the study of modern nanotechnology. In each of the examples that follow, it is clear that the direct determination of compositional information on a scale below 1000 nm (and often below 100 nm) is readily attainable using high resolution imaging SIMS. This capability sets the stage for exciting possibilities in many areas of nanotechnology such as MEMS, nanosensors, nanomedicine, and more.

4.1. Example—Precipitate Distributions in Metallurgy

The performance of metallurgical systems is often dependent on the microstructure and microchemistry present in the material at hand. The relevant length scales of these properties can range from a few angstroms to many millimeters. Very often, light elements such as boron, nitrogen, oxygen, and carbon are added as critical alloying elements to enhance strength, toughness, or corrosion resistance of steels. For example, the unwanted segregation of certain species into precipitates or grain boundaries can degrade the performance of an alloy. Imaging SIMS is uniquely qualified as a tool to map these compositional distributions, for any element, including hydrogen. In instruments such as the N50, these distributions can now be determined with resolutions that permit meaningful comparisons with data obtained from transmission electron microscopy thus permitting improved correlation of composition with microstructure. In some high resolution imaging SIMS instruments, it is also possible to generate ion-induced secondary electron images simultaneously with secondary ion images. The sputter process also provides grain or relief contrast that can be used to advantage for the metallurgist, even in alloys that are difficult to relief etch using traditional wet chemical metallurgical etches. In these cases, the secondary electron image can often provide perfect positional correlation of microstructure with composition.

An example of SIMS compositional imaging with simultaneous secondary electron imaging is given in figure 3(a–c). The sample is a welded steel alloy forging that was examined using a Cameca N50 using a 16keV Cs^+ primary beam, with negative secondary ion detection. The sample was sectioned, mounted in a tin-bismuth, low melting point eutectic alloy, and mechanically polished to provide a cross-sectional view of the material [52].

The formation of numerous fine precipitates is seen. In this particular data set, given the pixel density (125 nm/pixel) and probe size used (100 nm), precipitates as small as 250 nm are readily revealed. Here, conservative sampling is employed, where 2 pixels/feature (in any one direction) are assumed to be the minimum sampling level

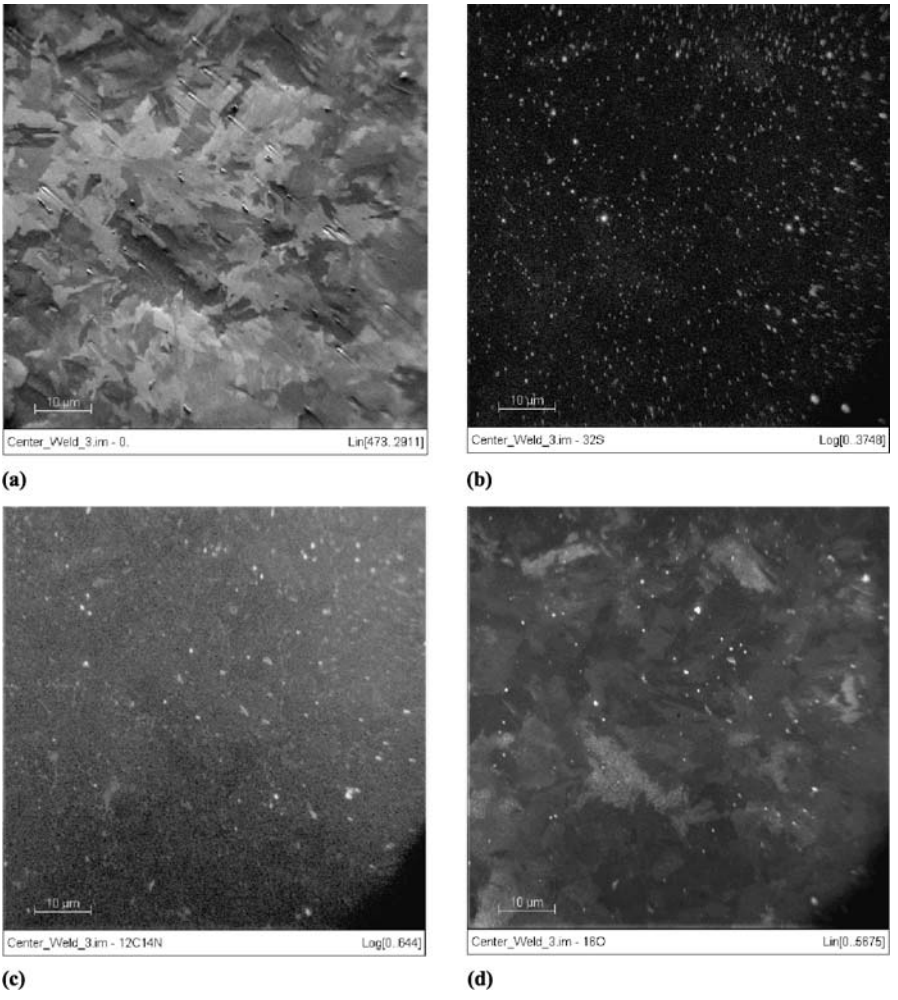

Figure 3. (a) Ion-induced secondary electron image of steel forging in welded zone, showing useful microstructural features. (Cameca N50, 16 keV Cs^+ primary ions). (b) SIMS ion image of sulfur ($32S^-$). Extensive precipitate formation detected, with 250 nm phases readily revealed. Composition is directly correlated with microstructure at left. (c) SIMS ion image of nitrogen ($26CN^-$). Evidence suggests that nitrogen is distributed both in solid solution and as precipitates. (d) SIMS ion image of oxygen ($16O^-$). Oxygen also seems to be distributed both in solid solution and as precipitates. Grain orientation effects are evident.

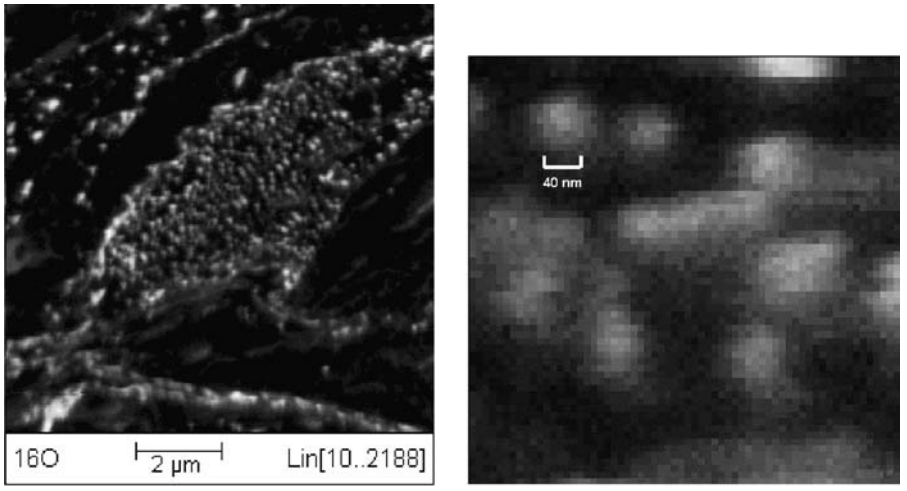

Figure 4. (a) SIMS ion image of copper grains. $16O^-$ image showing trace (bulk, ppm) distribution of copper in mechanically deformed grains. (Cameca N50, 16 keV Cs^+ primary ions). (b) Zoomed view from $16O^-$ ion image at left. Precipitate spacings well below 50 nm are clearly resolved, with precipitates on the order of 40 nm detected.

required to define a given feature [53]. As in any analysis, the analyst must strike a compromise between analyzed area, pixel density, dwell time, spatial resolution, and analysis time.

An example of higher resolution data is shown in figure 4(a–b). In this example, an 'oxygen free' copper alloy was being examined for trace oxide distributions. The sample at hand was mechanically deformed copper powder. Physical deformation occurred due to high-speed (supersonic) impact of the copper grains onto a substrate. The extreme sensitivity of dynamic SIMS in the N50 proved critical here, as both electron microprobe and TEM were unable to perform a successful analysis. Individual grains are revealed, with original grain boundaries and extent of plastic deformation apparent. Features below 50 nm are clearly resolved [54].

4.2. Example—Heterogeneous Catalyst Studies

Heterogeneous catalysis is a commercially important application area for the petrochemical industry where imaging SIMS has been applied. For example, extensive use of imaging SIMS has been made in the area of fluid catalytic cracking ("FCC") [55]. Modern FCC catalysts contain a complex mixture of submicron phases such as zeolites, clay, bulk alumina and a silica or alumina binder. From the perspective of nanotechnology, FCC catalysts can be considered as highly engineered nanoscale ceramics. From the perspective of SIMS, these systems are challenging due to their inherent compositional complexity and electrical insulating properties.

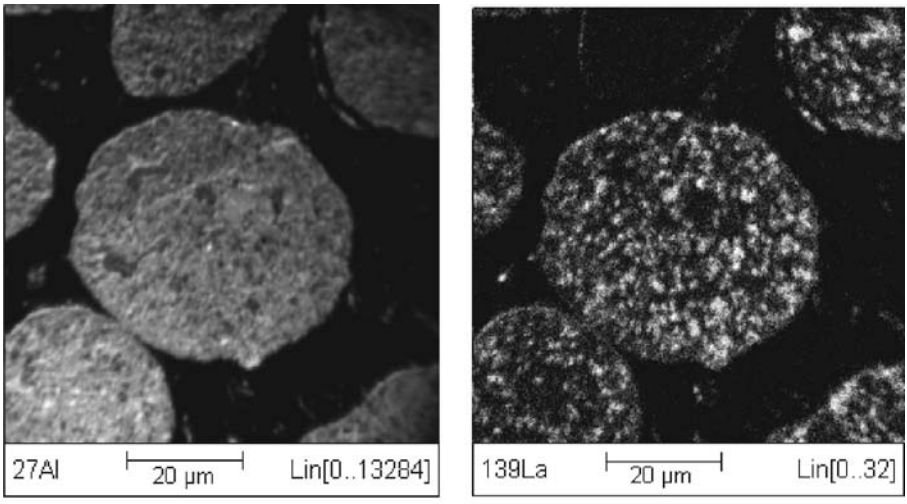

Figure 5. (a) Lower magnification aluminum SIMS ion image ($27AI^+$) of FCC catalyst particles as viewed in cross section. Submicron resolution is preserved. (Cameca N50, 16 keV O^- primary ions). (b) Corresponding rare earth map ($139La^+$) showing position of zeolite phases throughout each FCC particle. Zeolites are intentionally doped with rare earth species to enhance hydrothermal stability.

As a first order approximation, the most important phase in FCC catalysis is the zeolite, which can be rendered inactive in use due to the accumulation of trace poisons such as nickel or vanadium, even at levels as low as a few ppm. The ability of imaging SIMS to identify and quantify the levels of poisons and other species on zeolites is obviously critical. Extending this capability to the complex mixture of nanoscale phases is truly a powerful tool in studying these systems.

Imaging SIMS data obtained on a typical FCC catalyst is shown in figure 5(a–b) [56]. Silicon and aluminum are contained in all phases, although at different concentrations. Silicon to aluminum difference images (or ratio images) can thus be used to effectively discriminate between the major phases. In order of decreasing silicon to aluminum ratio, we have the following typical progression: silica binder > zeolite > clay > bulk alumina or alumina binder. Note that the binder is usually either a pure silica or alumina. In addition to silicon to aluminum ratio, other trace species can often aid the analyst in major phase identification. For example, zeolites often intentionally contain rare earth species as stabilizers (i.e. lanthanum, cerium, etc). Similarly, clays are often uniquely identified by species such as titanium, iron, or calcium.

In figure 5 above, the catalyst particles have been embedded into epoxy and polished to reveal random cross sections. The particles are generally spherical, with diameters ranging between 40–100 um. Aluminum (viewed here as $27AI^+$) identifies the overall particle location. The lanthanum image ($139La^+$) gives a clear view of the zeolite distribution throughout the particles.

Using the oxygen primary beam, the N50 resolution is limited to approximately 150 nm. For higher resolution imaging, the cesium source is preferred (50 nm resolution attainable routinely) but can have some difficulty with charge compensation on difficult insulators. As can be seen in figure 6(a–f) below, high resolution data can be obtained on these catalyst samples, despite their electrical insulating properties. Features as small as 50 nm are clearly resolved. Simple image arithmetic provides a convenient tool for phase discrimination based upon appropriate compositional criteria such as silicon to aluminum ratio [57]. Color overlays as shown in figure 6(f) enable the rapid, qualitative determination of phase relationships.

Once the phases of interest have been discriminated, the use of binary masks enables the subsequent image analysis of compositional and morphological trends for these phases. For example, percent loading of zeolite within a catalyst can be readily calculated, as can the degree of poison pickup directly on to the zeolite phase versus other phases. The reader is referred to the work of Leta, *et al.* for details on the quantitative approach employed in this system [58].

4.3. Example—Nanoscale Biological Structures

One exciting area of research utilizing high resolution imaging SIMS involves the use of stable isotopic tracers to track biological activity within organisms [59]. Many biological structures possess both mechanical and chemical properties that serve as excellent analogues to the world of nanotechnology and are nano-scale in size [60].

One recent study of melanin granules within mammalian hair shafts demonstrates the utility of high resolution elemental SIMS imaging in these systems [61]. Compositional information from sub-100 nm structures within the hair shaft was readily obtained. Terrestrial isotope ratios for sulfur species were measured in the cuticle and cortex, demonstrating the additional possibility for isotopic tagging studies with a spatial resolution below 100 nm.

In a separate study, the distribution of iodo-benzamide melanoma markers within the cell ultrastructure has been studied successfully via high resolution imaging SIMS [62]. Here, the iodo-benzamide marker is used as a diagnostic tool for the detection of cancerous cells. The iodine ion ($^{127}I^-$) was detected only in the melanosomes, and not in other structures within the cells (figure 7). This confirms the suspected preferential uptake of this molecule as a marker for cancerous cells. This also demonstrates the potential utility of imaging SIMS in the development of therapeutic agents to attack specific cancerous structures.

5. SUMMARY AND FUTURE PERSPECTIVES

Recent improvements in instrumental performance have brought imaging SIMS well into the nano-regime. The ability to map trace compositional information for structures below 100 nm is now routinely possible. In order to take full advantage of these new technologies, it is important for the analyst to learn from the extensive traditional SIMS knowledge base that already exists. This is especially important as one attempts to determine optimal analytical protocols or quantify observations.

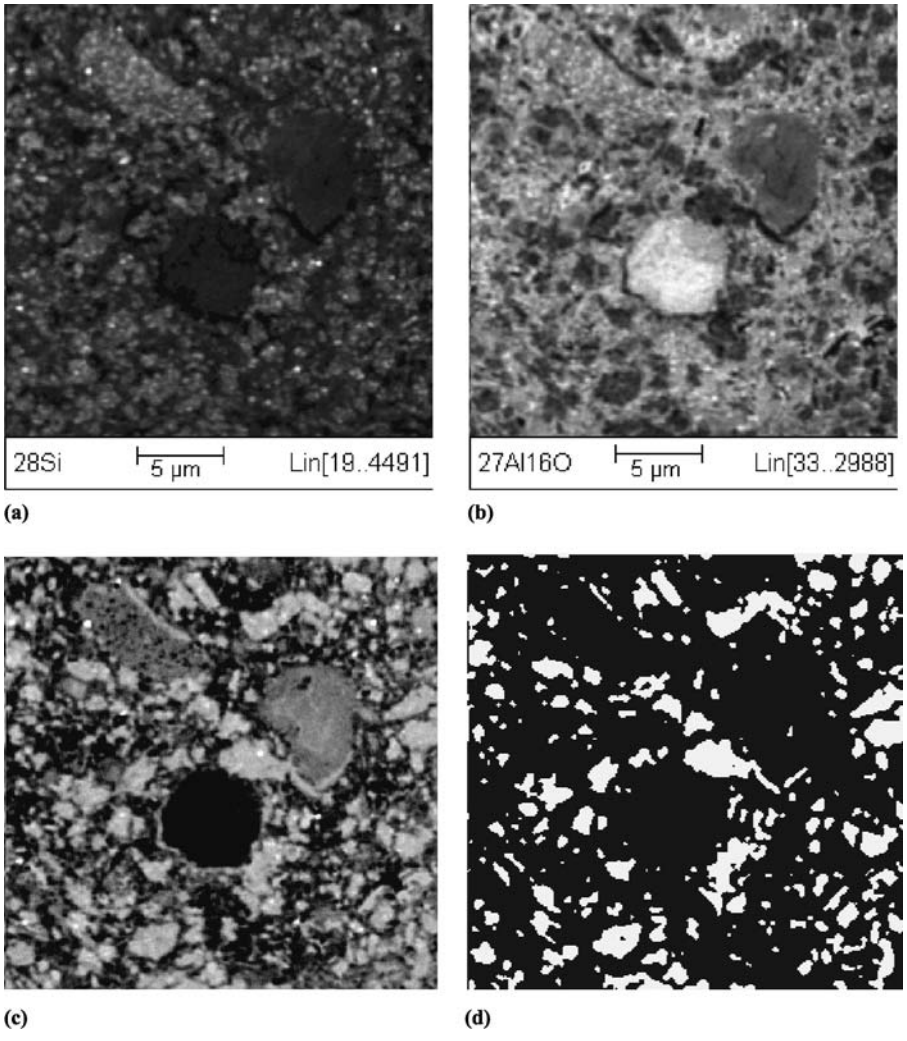

Figure 6. (a) High resolution silicon SIMS ion image ($28Si^-$) of FCC catalyst interior with 50 nm phases revealed. (Cameca N50, 16 keV Cs^+ primary ions). (b) High resolution aluminum SIMS ion image ($27Al16O^-$) of FCC catalyst interior. (c) Image processing methods can be used effectively to discriminate phases. Here, a silicon minus aluminum image (from 6a & 6b) reveals a complex phase map. (d) Simple binary map begins to define zeolite phases uniquely. Threshold function based upon silicon-aluminum intensities from image at left. Subsequent analysis can now reveal vanadium pickup on zeolite versus other phases. (e) Higher magnification image of $28Si^-$ demonstrates 50 nm phase identification. (f) Color overlay of $28Si^-$ (red) and $27Al16O^-$ (green) reveals fine scale phase relationships. (See color plate 4.)

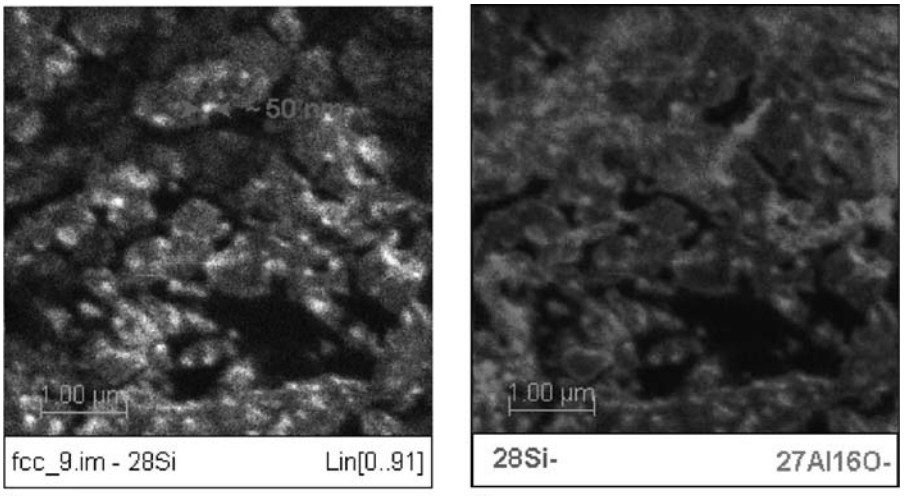

Figure 6. (continued)

Both dynamic SIMS and TOF SIMS instruments are highly developed from the point of view of mass spectrometry. Still, improvements continue to emerge. For example, the use of array detectors at the exit plane of a magnetic sector has the potential for enabling full-spectrum imaging within a limited mass range [64, 65]. Ion source development is proving to be critical in both TOF and magnetic sector SIMS, pushing the limits of resolution and sensitivity, as new source designs are explored [66].

The future of high resolution imaging SIMS is equally exciting as one looks towards the wide array of applications in many fields of science. The field of nanotechnology is starting to realize the utility of SIMS, as more instruments with high spatial resolution become available. It is widely recognized that ion-beam based instruments such as FIB tools are critical in the development of nanodevices. In a similar way, high resolution imaging SIMS is poised for applications in nanotechnology where one needs to probe the composition of fine structures, at trace levels, with isotopic specificity, and a spatial resolution on the order of 50–1000 nm.

REFERENCES

1. M. G. Dowsett, Proceedings of SIMSXI, p. 259–264. John Wiley & Sons. Orlando, FL (1997).
2. P. A. Ronsheim and K. L. Lee, Proceedings of SIMSXI, p. 301–304. John Wiley & Sons. Orlando, FL (1997).
3. F. Hillion, B. Daigne, F. Girard, G. Slodzian, Proceedings of SIMS IX, p. 254, John Wiley & Sons. Yokohama (1993).
4. S. Messenger, L. P. Keller, F. J. Stadermann, R. M. Walker, and E. Zinner, *Science*, 300 (2003) 105.

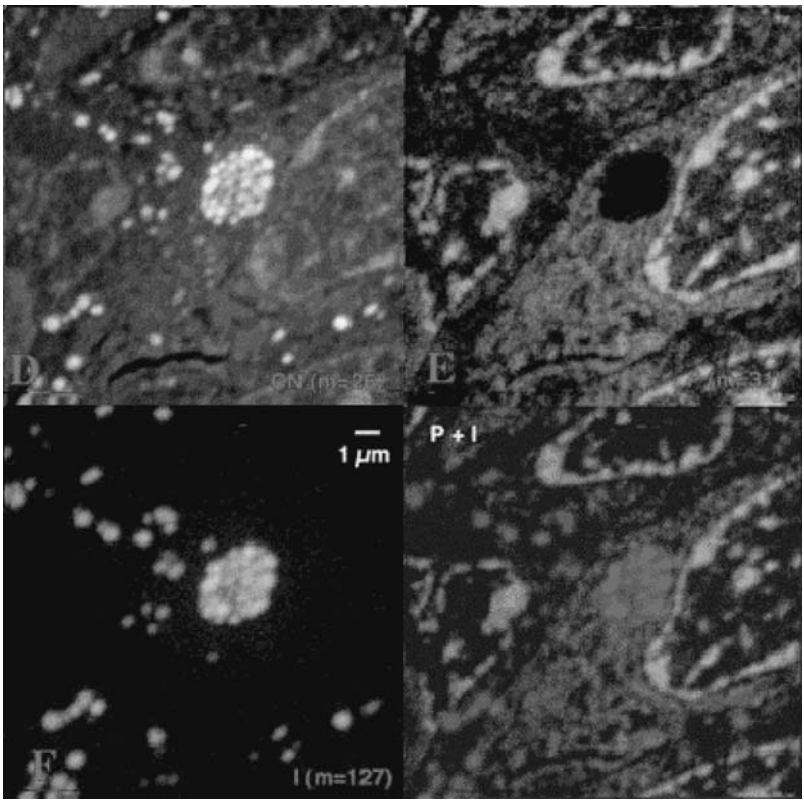

Figure 7. High resolution SIMS images of B16 melanoma cells from a mouse lung colony. Nitrogen (viewed as 12C14N- in frame "D") indicates overall cell structure. Phosphorus (31P- in frame "E") is present through the cell, being concentrated in the cell nucleus but absent from melanin. Iodine, present only in the marker, clearly targets the melanin. Reprinted with permission [63]. (See color plate 5.)

5. Z. Postawa, B. Czerwinski, M. Szewczyk, E. Smiley, N. Winograd and B. Garrison, *J. Phys. Chem*. B 2004.108.7831–7838.
6. Z. Postawa, B. Czerwinski, M. Szewczyk, E. Smiley, N. Winograd and B. Garrison, *Anal Chem*. (2003). 4402–4407.
7. S. V. Verkhoturov, E. A. Schweikert, and N. M. Rizkalla, *Langmuir*, 18 (2002) 8836–8840.
8. A. V. Hamza, T. Schenkel, A. V. Barnes, and D. H. Schneider, *J. Vac. Sci. Technol.* A 17(1) (1999) 303.
9. C. F. Klein and D. P. Leta, Proceedings of SIMSVII, p. 45–48. John Wiley & Sons. Monterey, CA (1989).
10. E. Hindié, Proceedings of SIMS XI, p. 113, John Wiley & Sons. Orlando, FL (1997).
11. M. W. Thompson, *Philos. Mag.* 18 (1968) 377.
12. P. Sigmund, *Phys. Rev.* 184 (1969) 383.
13. H. A. Storms, K. F. Brown, and J. D. Stein, *Anal. Chem*., 49 (1977) 2023.
14. C. A. Andersen, *Int. J. Mass Spectrom. Ion Phys.*, 3 (1970) 413.
15. M. L. Yu, *Physical Review Letters*, 40, No. 9, (1978) 574.
16. R. Smith, D. E. Harrison, Jr., B. J. Garrison. *Phys. Rev. B*, 40 (1) (1989) 93.
17. I. A. Wojciechowski, S. Sun, C. Szakal, N. Winograd, and B. J. Garrison, *J. Phys. Chem. A*, 108 (2004) 2993–2998.

18. R. G. Wilson, F. A. Stevie, and C. W. Magee, *Secondary Ion Mass Spectrometry—A Practical Handbook for Depth Profiling and Bulk Impurity Analysis, Wiley-Interscience, New York* (1989).
19. J. C. Vickerman, A. Brown, and N. M. Reed (Eds.), *Secondary Ion Mass Spectrometry, Principles and Applications. International Series of Monographs on Chemistry 17*. Clarendon Press, Oxford (1989).
20. M. L. Pacholski and N. Winograd, *Chem. Rev.* p. 2977–3005 (1999).
21. T. Stephan, *Planetary and Space Science*, 49 (2001) 859–906.
22. A. Wucher, S. Sun, N. Winograd, *Appl. Surf. Sci*. (2004) in press.
23. F. Kotter, E. Niehuis, and A. Benninghoven, Proceedings of SIMS XI, p. 459, John Wiley & Sons. Orlando, FL (1997).
24. A. Tempez *et al.*, *Rapid Commun. Mass Spectrom*., 18 (2004) 371–376.
25. ION-TOF GmbH, Gievenbecker Weg 15, 48149 Muenster, Germany.
26. PHI, Physical Electronics, Inc. 18725 Lake Drive East, Chanhassen, MN 55317.
27. J. Mattauch and R. Herzog, *Z. Physik*, 89 (1934) 786.
28. R. Levi-Setti, G. Crow, Y. L. Wang, N. W. Parker*, R. Mittleman, and D. M. Hwang, *Phys. Rev. Lett*. 54 (1985) 2615–2618.
29. L. Christman, presented at *8th Annual Workshop on Secondary Ion Mass Spectrometry*, Lake Harmony, PA (1995).
30. G. Slodzian, B. Daigne, F. Girard, F. Hillion, Proceedings of SIMS VIII, p. 169, John Wiley & Sons. Amsterdam (1991).
31. F. Horreard, presented at *17th Annual Workshop on Secondary Ion Mass Spectrometry*, Westminster, CO (2004).
32. F. Hillion, F. Horreard, F. J. Stadermann, Proceedings of SIMS XII, John Wiley & Sons. Brussels (1999).
33. H. A. Storms, K. F. Brown, and J. D. Stein, *Anal. Chem.*, 49 (1977) 2023.
34. R. G. Wilson, F. A. Stevie, and C. W. Magee, *Secondary Ion Mass Spectrometry—A Practical Handbook for Depth Profiling and Bulk Impurity Analysis, Wiley-Interscience, New York* (1989).
35. D. P. Leta and G. H. Morrison, *Anal. Chem.*, 52 (1980) 277.
36. G. L. Liu *et al.*, J. Vac. Sci. Technol. B14(1) (1996).
37. A. G. Borzenko, *et al.*, *Microscopy and Microanalysis*, 29–31 (Nov 1999).
38. W. C. Horn and W. A. Lamberti, *12th Annual Workshop on Secondary Ion Mass Spectrometry*, Gaithersburg, MD (1999).
39. D. P. Leta and G. H. Morrison, *Anal. Chem.*, 52 (1980) 277.
40. J. D. Ganjei, D. P. Leta, and G. H. Morrison, *Anal. Chem.*, 50 (1978) 285.
41. Ibid.
42. D. P. Leta and E. L. Kugler in *Characterization and Catalyst Development—ACS Symposium Series 411*, Chapter 32, p. 354 (1989).
43. D. P. Leta, W. A. Lamberti, M. M. Disko, E. L. Kugler, W. A. Varady, in *ACS Symposium Series 452—Advances in FCC Technology II*, Chapter 17, p. 269–292, (1991).
44. G. H. Morrison and S. Chandra. Proceedings of SIMS XI, p. 109, John Wiley & Sons. Orlando, FL (1997).
45. E. Hindie', Proceedings of SIMS XI, p. 113, John Wiley & Sons. Orlando, FL (1997).
46. C. W. Magee, W. L. Harrington, and E. M. Botnick, *International Journal of Mass Spectroscopy and Ion Processes*, 103 (1990) p. 45–46.
47. P. Willich and R. Bethke, Proceedings of SIMS XI, John Wiley & Sons. Orlando, FL (1998) p. 991–994.
48. T. Mootz, A. Adriens, and F. Adams, *International Journal of Mass Spectroscopy and Ion Processes*, 156 (1996) p. 1–10.
49. P. A. W. van der Heide, *et al.*, *Surface and Interface Analysis*, 21, (1994) pp. 747–757.
50. P. A. W. van der Heide, *Surface Science Letters*, 302 (1994) L312–L318.
51. R. Losing, N. Reger, F. J. Stadermann, and H. M. Ortner. Proceedings of SIMS XI, p. 1019, John Wiley & Sons. Orlando, FL (1997).
52. W. C. Horn and W. A. Lamberti, *17th Annual Workshop on Secondary Ion Mass Spectrometry*, Westminster, CO (2004).
53. C. E. Shannon, *The Bell System Technical Journal*, 27 (July, October 1948) p. 379–423, 623–656.
54. W. C. Horn and W. A. Lamberti, *17th Annual Workshop on Secondary Ion Mass Spectrometry*, Westminster, CO (2004).
55. E. L. Kugler, D. P. Leta, *J. of Catalysis*, 109, (1988) 387.
56. W. A. Lamberti and W. C. Horn, *17th Annual Workshop on Secondary Ion Mass Spectrometry*, Westminster, CO (2004).
57. Ibid.

58. D. P. Leta, W. A. Lamberti, T. E. Clark, W. A. Varady. Proceedings of SIMS VIII, John Wiley & Sons. (1992) p. 541.
59. Peteranderl, R. and C. Lechene. *Journal of The American Society for Mass Spectrometry*. In press.
60. Pickles, J., *V. Mechanisms of transduction and excitation in the cochlea. An Introduction to the Physiology of Hearing*. Academic Press. 107–153 (1982).
61. Hallegot, P., R. Peteranderl and C. Lechene, *Journal of Investigative Dermatology*. 122 (2004) 381–386.
62. J. Guerquin-Kern, F. Hillion, J. Madelmont, P. Labarre, J. Papon, and A. Croisy, *Biomedical Engineering Online* 2004, 3:10. (http://www.biomedical-engineering-online. com/content/3/1/10).
63. Copyright © 2004, Guerquin-Kern *et al*.; licensee BioMed Central Ltd. This is an Open Access article: verbatim copying and redistribution of this article are permitted in all media for any purpose, provided this notice is preserved along with the article's original URL: (http://www.biomedical-engineering-online. com/content/3/1/10). Biomed Eng Online. 2004; 3 (1): 10.
64. Barnes IV, J. H., Schilling, G. D., Sperline, R. P., Denton, M. B., Barinaga, C. J., Koppenaal, D. W., and Hieftje, G. M., *J. Am. Soc. for Mass. Spectrom*., (2004). (In Press).
65. J. Barnes, R. Sperline, M. B. Denton, C. Barinaga, D. Koppenaal, E. Young, and G. Hieftje, *Anal. Chem*., (2002) 74 (20), 5327–5332.
66. Guillermier, C., C. P. Lechene, J. Hill and F. Hillion. *Review of Scientific Instruments*. 74, (2003) 3312–3316.